www.sciencemag.org/content/360/6391/eaan5931/suppl/DC1

# Supplementary Materials for

## Gut microbiome–mediated bile acid metabolism regulates liver cancer via NKT cells

Chi Ma, Miaojun Han, Bernd Heinrich, Qiong Fu, Qianfei Zhang, Milan Sandhu, David Agdashian, Masaki Terabe, Jay A. Berzofsky, Valerie Fako, Thomas Ritz, Thomas Longerich, Casey M. Theriot, John A. McCulloch, Soumen Roy, Wuxing Yuan, Vishal Thovarai, Shurjo K. Sen, Mathuros Ruchirawat, Firouzeh Korangy, Xin Wei Wang, Giorgio Trinchieri, Tim F. Greten*

*Corresponding author. Email: tim.greten@nih.gov

Published 25 May 2018, *Science* **360**, eaan5931 (2018)
DOI: 10.1126/aan5931

**This PDF file includes:**

## Materials and Methods

Murine studies

SPF C57BL/6 and BALB/c mice were purchased from Charles River. CXCR6 knockout mice were purchased from Jackson laboratory. CD1d knockout mice, LAP-tTA and TRE-MYC mice have been previously described (*10*). Germ-free mice were provided by Dr. Romina Goldszmid (Cancer and inflammation program, NIH). Newly purchased four-week old C57BL/6 or BALB/c mice were randomized into 5 mice/cage and housed for one week to normalize gut microbiome. Then mice were assigned into H2O or ABX treatment groups. Mice in the ABX group received three-antibiotic cocktail in the drinking water containing vancomycin (Hospira, 0.5g/L), neomycin (VETone, 0.5g/L) and primaxin (Merck&CO, 0.5g/L) as previously reported (*3*). In some experiments mice were given single antibiotic water, and cefoperazone (MP Biomedicals) was given at the concentration of 0.5g/L. Fresh antibiotic water was replaced every other day. After 3 weeks of ABX pretreatment, mice were challenged with different tumor cell lines. B16-F1 and A20 cells were purchased from ATCC. EL4 cells were used as described (*37*). $1x10^6$ EL4 tumor were given by *s.c.* or tail vein injection, $3 x10^5$ B16-F1 tumor cells were given by intrasplenic injection as described before (*11*), and $1x10^6$ A20 tumor cells were given by tail vein injection. In some experiments mice were fed with a 2% cholestyramine diet made by Research Diets Inc (New Brunswick, NJ). Mice were treated with 500 μg anti-CD4 (clone GK1.5, BioxCell) or 200 μg anti-CD8 (clone 2.43, BioxCell) 24 hrs before receiving tumor injection for depletion studies. For *in vivo* NKT cell stimulation, $1x10^6$ αGalCer-loaded A20 tumor cells in the combination of brefeldin A (500 ug/mouse) were given by tail vein injection, and mice were sacrificed 3 hrs after injection. αGalCer-loading was performed by incubate A20 cells with 1 μg/ml αGalCer overnight followed by 3 times of washing. At the experimental end points, mice were sacrificed for organ harvest. All experiments were conducted according local institutional guidelines and approved by the Animal Care and Use Committee of the National Institutes of Health, Bethesda, USA.

Flow cytometry

Cells were surface-labelled with the indicated antibodies for 15 min at 4 °C. Intracellular staining using a Foxp3/transcription factor staining buffer set (eBioscience) was used according the manufacturer's instructions. Flow cytometry was performed on a BD LSRFortessa platform and results were analyzed using FlowJo software version 9.3.1.2 (TreeStar). Dead cells were excluded by using live/dead fixable near-IR dead cell staining kit (ThermoFisher scientific). The following antibodies were used for flow cytometry analysis: anti-TCRβ-BV510 (clone H57-587, Biolegend), PBS57/CD1d-tetramer-APC (NIH core facility), anti-CXCR6-FITC (clone SA051D1, Biolegend), anti-CD3-PE (clone 17A2, Biolegend), anti-CD4-PE (clone RM4-5, Biolegend), anti-CD4-Alexa Fluor 700 (clone GK1.5, Biolegend), anti-CD8-BV210 (clone 53-6.7 Biolegend), anti-CD19-PerCP/Cy5.5 (clone eBio1D3, eBioscience), anti-CD49b (clone DX5, eBioscience), anti-TCRγ/δ-PE, (clone GL3, BD pharmigen), anti-CD11b-BV421 (clone M1/70, Biolegend), anti-Ly6G-Alexa Fluor 700 (clone 1A8, Biolegend), anti-Ly6C-APC (clone HK1.4, Biolegend), anti-CD44-PE/Cy7 (clone IM7, eBioscience), anti-CD62L-PerCP/Cy5.5 (MEL-14, Biolegend), anti-CD69-Pacific blue (clone H1.2F3, Biolegend),

anti-CD25-FITC (clone 7D4, BD pharmigen), anti-4-1BB-PE (clone 17B5, Biolegend), anti-Foxp3-Alexa Fluor 488 (clone 22F6, Biolegend), anti-Tbet-Pacific Blue (clone 4B10, Biolegned), anti-RORγ-PE (clone B2D, eBioscience), anti-PLZF-PerCP/Cy5.5 (clone 9E12, Biolegend), and anti-CD1d-PE (clone 1B1, eBioscience), anti-IFNγ-PE (clone XMG1.2, BD Biosciences), anti-TNFα-PerCP/Cy5.5 (clone MP6-XT22, Biolegend). The following markers were used for identifying different immune cell subsets: $TCR\beta^+CD1d\text{-}Teteramer^+$ for NKT cells, $CD3^+CD4^{hi}$ for hepatic $CD4^+$ T cells, $CD3^+CD8^+$ for $CD8^+$ T cells, $CD3^-CD19^+$ for B cells, $CD3^-CD49b^+$ for NK cells, $CD3^+TCR\gamma/\delta^+$ for γ/δ T cells, $CD11b^+Ly6G^+Ly6C^{lo}$ for G-MDSC. Absolute numbers were calculated by multiplying frequencies obtained from flow cytometry by the total live mononuclear cell count, and then divided by liver weight.

*In vivo* cytotoxcicity assay

Splenocytes isolated from naïve C57BL/6 mice were loaded with αGalCer (1 μg/ml) then labelled with high dose of CFSE as target cells. Unloaded cells were labelled with low dose of CFSE as control cells. Then $CFSE^{hi}$ target cell and $CFSE^{lo}$ controls cells were mixed at about 1:1 ratio. $10^7$ mixed cells were injected *i.v.* into ABX or H2O-treated C57BL/6 mice. Sixteen hours later, mice were killed and cytotoxicity was analysed by flow cytometry. $r=(\%CFSE^{lo} / \%CFSE^{hi})$; $r_o$ is the ratio of mixed cells without injection; % cytotoxicity=$[1- (r_0/r) ]x100$.

Immunohistochemistry and Quantification

Immunohistochemistry was performed on 3 μm sections obtained from formalin-fixed paraffin-embedded liver tissues of H2O (n=5) or ABX (n=5) treated mice using the Opal™ 5-color IHC Kit (PerkinElmer, Waltham, MA, USA) according to the manufacturer´s instructions. The following primary antibodies were used: anti-CXCL16 (Bioss Antibodies, Woburn, MA, USA; bs-1441R, rabbit polyclonal, 1/4.000, Opal 620), anti-LYVE1 (Abcam, Cambridge, UK; rabbit polyclonal, 1/15.000, Opal 520). Slides were evaluated using the Vectra® 3 automated, high-throughput quantitative pathology imaging system (PerkinElmer) and the inForm® software (PerkinElmer) for segmentation and quantification of $CXCL16^+/LYVE1^+$ cells.

Hepatic bile acid profiling

Fresh mice liver tissue was snap frozen in liquid nitrogen and then kept at -80 $^oC$. Hepatic bile acid composition was measured at West Coast Metabolomics Center at UC Davis using the targeted metabolite analysis service.

Liver sinusoidal endothelia cell preparation and bile acids treatment

Primary mice liver sinusoidal endothelia cells were isolated as previously described (38). Briefly, mice were CO2 euthanized, and then the portal vein was cannulated and the liver was perfused with 0.05 % collagenase in $Ca^{2+}$ deprived medium. Liver cells were dissociated and parenchymal cells were killed by incubation in 0.04 % collagenase in Gey's balanced salt solution at 37 $^oC$ for 15 minutes. Then density gradient centrifugation was performed using Nycodenz solution at the final solution of 1.089 $g/cm^3$. LSECs were isolated using anti-LSEC microbeads (Miltenyi) according to the manufacturer's instructions. LSECs or the human SK-HEP1 cell line (ATCC, HTB-52) were treated

with different bile acids for 24 hours. Gene expression was analyzed by real-time PCR. TCA, CDCA, DCA, and TDCA were purchased from Sigma. T-β-MCA, ω-MCA, and T-ω-MCA were purchased from Steraloids Inc.

*In vivo* bile acids feeding

Mice were kept on ABX cocktail and fresh ABX was replaced every other day. Mice were fed with bile acids by oral gavage 48, 24 and 16 hrs prior to sacrifice. For A20 tumor bearing mice, ω-MCA, LCA or CDCA were given 3 times/week. Bile acids were dissolved in corn oil. ω-MCA and CDCA were given at the dose of 6 mg/15g body weight, LCA was given at the dose of 1 mg/15g body weight.

Adoptive transfer of NKT cells.

Donor NKT-rich cells were isolated from livers of wild-type C57BL/6 mice by autoMACs sorting of $NK1.1^+$ cells. Half million of NKT-rich cells were transferred into $CXCR6^{-/-}$ mice by tail vein injection. Two days later mice were scarified and the liver accumulation of transferred NKT cells were measured by flow cytometry as $TCR\beta^+CD1d\text{-}Teratmer^+CXCR6^+$ population.

Gut colonization with Clostridium scindens.

Mice were fed with vancomycin in drinking water (Hospira, 0.5g/L) for one week. Fresh antibiotic water was replaced every other day. One week later vancomycin was stopped, and the mice were given oral gavage of $10^9$ *C. scindens* or vehicle (anaerobic glycerol) every day for 5 days. *C. scindens* was purchased from ATCC (35704), and grown under anaerobic conditions. One day after gavage, the colonization of *C. scindens* were confimed by real-time PCR using primers specific for C. scindens. For A20 tumor study, BALB/c mice were fed with vancomycin for one week. Then vancomycin was stopped, and A20 tumor ($1x10^6$ cells) were injected i.v. Mice were given oral gavage of $10^9$ *C. scindens* or *C. innocuum* (ATCC 14501) every day for 4 days. Then mice were given a second round of vancomycin treatment for 4 days, followed by additional four days of oral gavage of *C. scindens* or *C. innocuum*. Fourteen days after tumor injection, mice were sacrificed and liver tumor burden was measured.

16S rRNA sequencing and analysis

Mouse stool DNA extraction and 16S V4 tregion amplification were performed on the liquid handling robots (Eppendorf, epMotion5075 and epMotion 5073). The V4 region of the 16S rDNA gene (515F-806R) was sequenced; generating partially overlapping, paired-end reads on the Illumina MiSeq platform. After quality control filtering; a total of 3,979,728 reads were processed with an average of 132,657 reads per sample. The demultiplexed FASTQ files containing the 16S rRNA gene sequences were filtered for chimeric sequences using the USEARCH (version 8.1.1831) utility's UCHIME implementation and the 'gold' database (version microbiomeutil-r20110519). The reads were then binned into Operational Taxonomic Units (OTUs) at 97% similarity using USEARCH's cluster_otus command. The OTUs thus obtained were classified and aligned using QIIME (1.9.1) scripts. The assign_taxonomy.py script was used to assign taxonomy using the default RDP method and the default GreenGenes database. This provided insight into the larger trends at higher taxonomic levels (such as order

*Clostridiales*). The 16S rRNA sequencing data was deposited into Sequence Read Archive (SRA) public database with the accession number SRP136953.

Human studies

Non-tumor specimens derived from a set of 142 patients of the TIGER-LC Consortium were used in this study (*34*). Transcript expression was measured using the Affymetrix Human Transcriptome Array 2.0. Data has been deposited into the Gene Expression Omnibus (GEO) public database at NCBI (GEO Series GSE76297). A total of 718 biochemical metabolite species were measured by Metabolon's Discover HD4 Platform. All expression and metabolite data were log2 transformed. Pearson correlation analysis was performed using GraphPad Prism 7 to determine correlation between CXCL16 gene expression and selected metabolites. Due to the missing information cuased by detection limitations, 85 valid patient data were used to correlate CDCA and CXCL16 expression.

Statistical analysis

The sample sizes for animal studies were guided by previous murine studies in our laboratory. Statistical analysis was performed with GraphPad Prism 7 (GraphPad Software). The significant differences between groups were calculated by Student's unpaired t-test, one-way, or two-way ANOVA (Tukey's and Bonferroni's multiple comparison test). Welch's corrections were used when variances between the groups were unequal. $P < 0.05$ was considered as statistically significant.

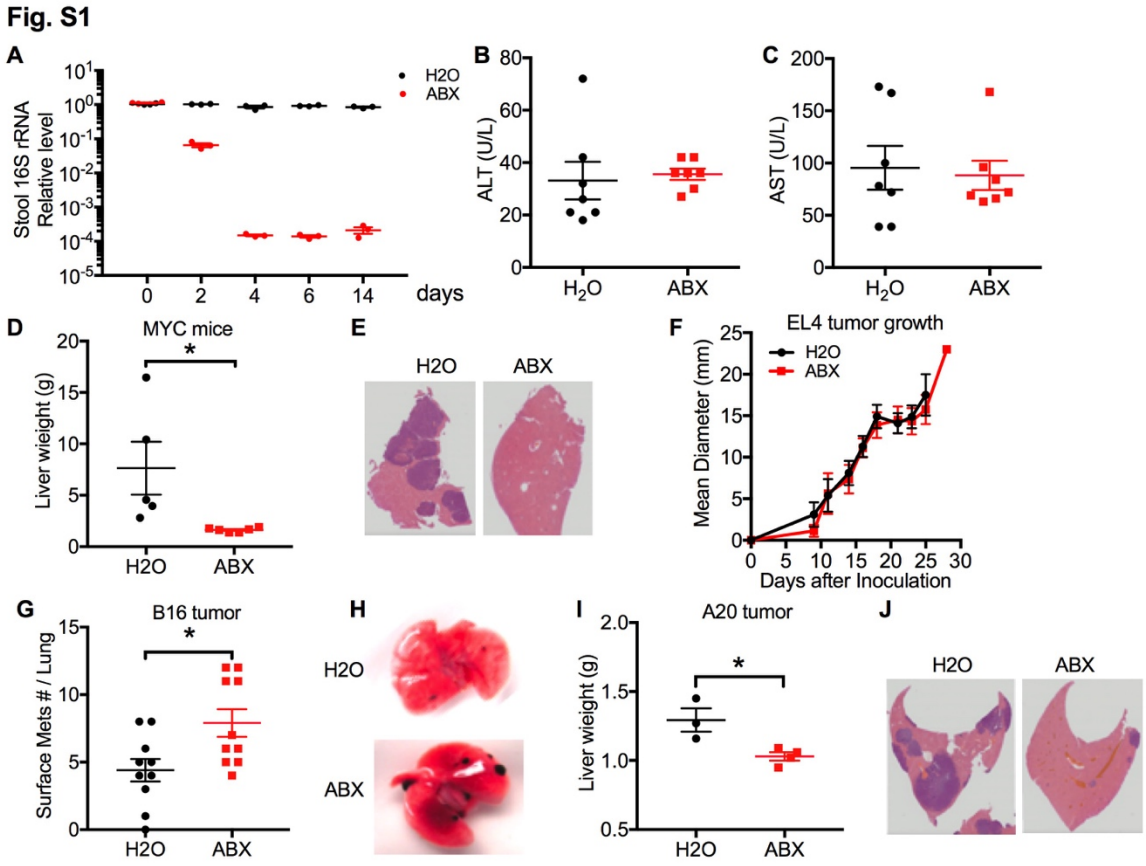


**Fig. S1.**

Removing gut commensal bacteria inhibits liver tumor growth. (A) The efficacy of ABX to remove gut bacteria was confirmed by quantifying stool bacterial load using real-time PCR to detect 16S rRNA gene. Data represent mean ± SEM of two pooled experiments. (B, C) Serum ALT and AST levels in mice treated with ABX or H2O. Data represent mean ± SEM of two pooled experiments. n=7. (D, E) Liver weight and representative H&E staining of liver sections of the MYC-ON mice described in Figure 1A. Data represent mean ± SEM of two pooled experiments. n=5 for H2O, 6 for ABX. $p<0.05$, Student's t-test. (F) Growth curve of *s.c.* EL4 tumors in mice treated with ABX or H2O. n=5. (G, H) ABX or H2O pretreated mice were given tail vein injection of B16 tumor cells. Lung metastasis was measured. Data represent mean ± SEM of two pooled experiments. n=10, $p<0.05$, Student's t-test. (I, J) Liver weight and representative H&E staining of liver sections in mice received tail vein injection of A20 tumor cells. n=4, $p<0.05$, Student's t-test.

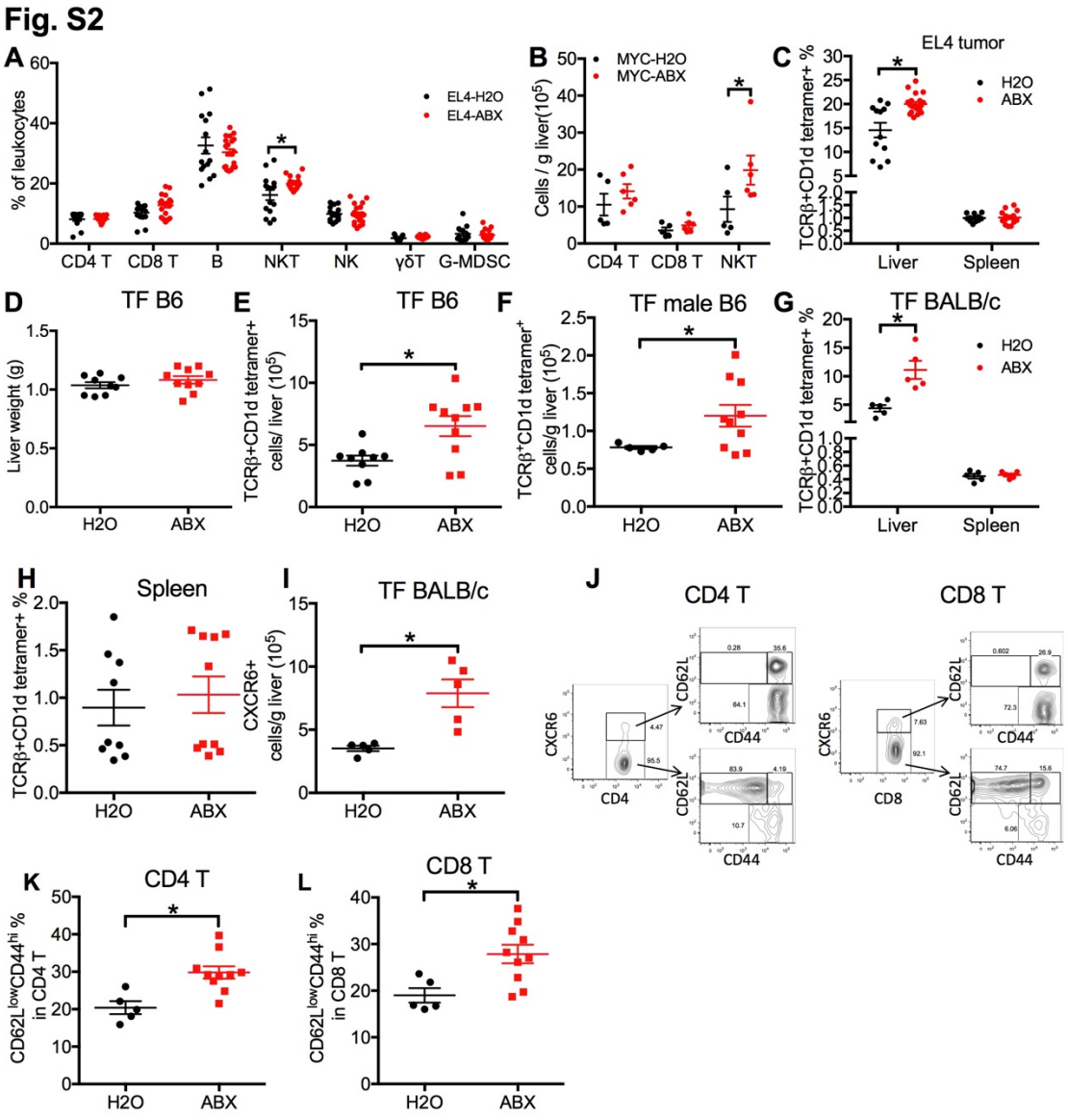


**Fig. S2**

Depleting gut commensal bacteria increases hepatic NKT cells. (A) Frequencies of immune cell subsets in liver infiltrating mononuclear cells from EL4-tumor bearing mice treated with ABX or H2O described in Figure 2A. Data represent mean ± SEM of three pooled experiments. n=15 for EL4-H2O, 20 for EL4-ABX. $p<0.05$, two-way ANOVA. (B)Absolute numbers of hepatic NKT, CD4 T and CD8 T cells in MYC mice described in Figure 1A. Data represent mean ± SEM of two pooled experiments. n=5 for H2O, 6 for ABX. $p<0.05$, two-way ANOVA. (C) Frequencies of NKT cells in the liver and spleen of EL4 tumor-bearing mice treated with ABX or H2O. n=15 for EL4-H2O, 20 for EL4-ABX. $p<0.05$, two-way ANOVA. (D, E) Liver weight and hepatic NKT cell absolute number per liver of C57BL/6 mice treated with ABX or H2O for 3 weeks. Data represent mean ± SEM of two pooled experiments. n=9 for H2O, 10 for ABX, $p<0.05$, Student's t-

test. (F) Male C57BL/6 mice were fed with ABX or H2O. Hepatic NKT cells were measured. Data represent mean ± SEM of two pooled experiments. n=5 for H2O, 10 for ABX. $p<0.05$, Student's t-test. (G) Frequencies of NKT cells in the liver and spleen of tumor-free BALB/c mice treated with ABX or H2O. n=5, $p<0.05$, two-way ANOVA (H) Frequencies of NKT cells in the spleen of naïve C57BL/6 mice. Data represent mean ± SEM of two pooled experiments. n=9 for H2O, 10 for ABX. (I) $CXCR6^+$ liver infiltrating mononuclear cells in tumor-free BALB/c mice after ABX or H2O treatment. Data represent mean ± SEM of two pooled experiments. n=5, $p<0.05$, Student's t-test. (J) Representative CD44 and CD62L staining of $CXCR6^+$ CD4 or CD8 T cells in liver. (K, L) Frequency of effector/memory CD4 Tor CD8 T cells in liver of tumor-free C57BL/6 mice treated with ABX or H2O. Data represent mean ± SEM of two pooled experiments.

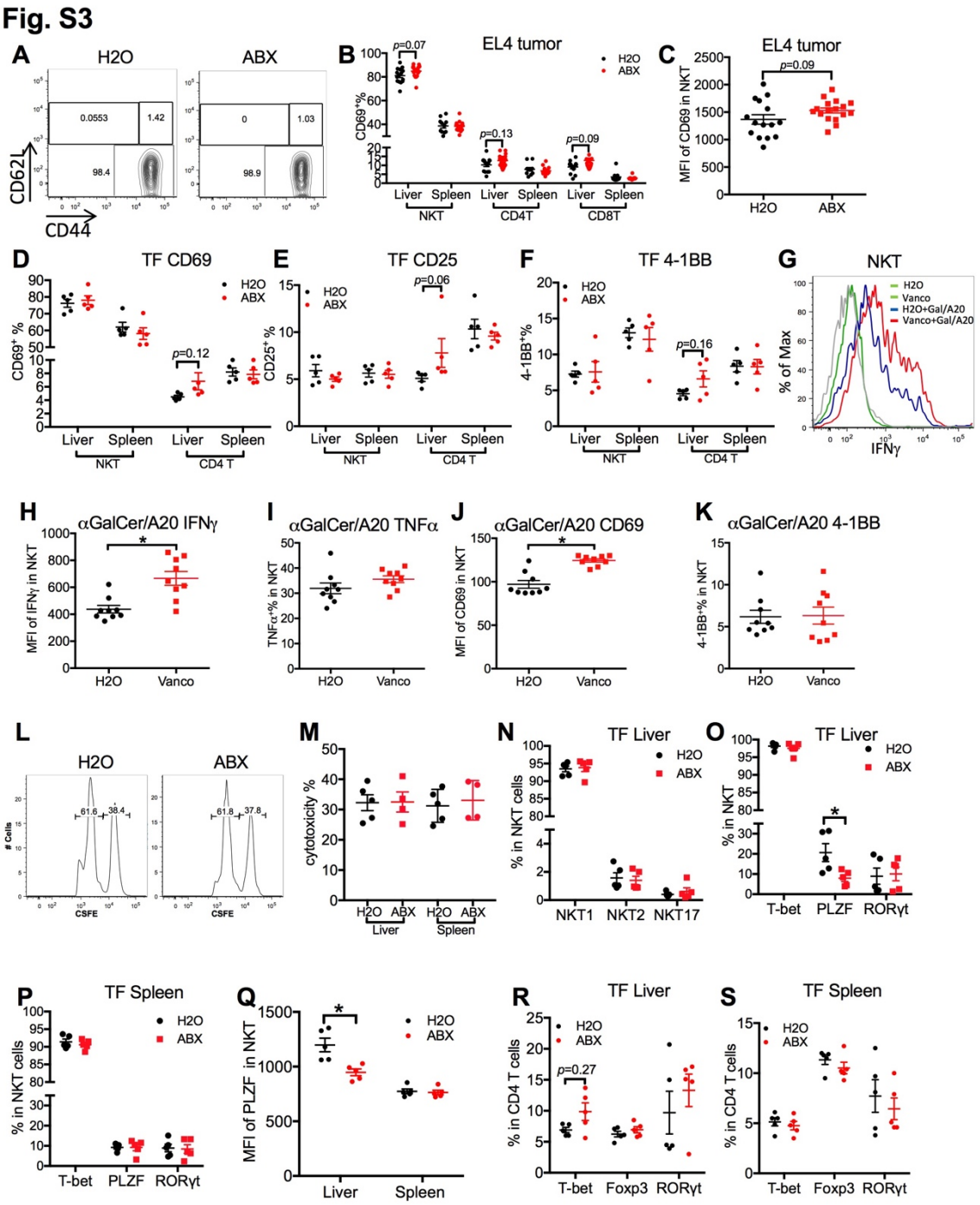


**Fig. S3**

Phenotyping NKT cells and CD4 T cells after removing gut commensal bacteria. (A) Representative CD44 and CD62L staining of hepatic NKT cells. (B) Frequencies of $CD69^+$ NKT, CD4 T and CD8 T cells in the liver and spleen from EL4-tumor bearing mice. Data represent mean ± SEM of three pooled experiments. n=15 for EL4-H2O, 20 for EL4-ABX. (C) MFI of CD69 in hepatic NKT cells is shown. Data represent mean ± SEM of three pooled experiments. n=15 for H2O, 18 for ABX. (D, E, F) $CD69^+$, $CD25^+$,

and 4-1BB$^{+}$ levels of NKT and CD4 T cells in liver and spleen from tumor-free C57BL/6 mice. n=5, two-way ANOVA. (G, H, I, J, K) BALB/c mice fed on vancomycin or H2O were given *i.v.* injection of $10^{6}$ α-galactosylceramide-loaded A20 tumor cells (Gal/A20) in the combination of brefeldin A (500 μg/mouse). Three hours later IFN-γ (G, H), TNF α (I), CD69 (J) and 4-1BB(K) were measured by flow cytometry. n=9, $p<0.05$, Student's t-test. (L, M) *In vivo* cytotoxicity analysis of NKT cells of ABX-or H2O treated mice. Representative histogram of CFSE-labelled cells isolated from livers 16 hrs after injection were shown (L). Quantification was shown in M. n=5 for H2O, 4 for ABX. (N) NKT1 (T-bet$^{hi}$PLZF$^{lo}$), NKT2(T-bet$^{lo}$PLZF$^{hi}$), and NKT17(T-bet$^{lo}$PLZF$^{int}$) levels in hepatic NKT cells are shown. (O, P) T-bet$^{+}$, PLZF$^{+}$, and RORγ$^{+}$ level of NKT cells in the liver or spleen of tumor-free C57BL/6 mice after ABX or H2O treatment. n=5, $p<0.05$, two-way ANOVA. (Q) MFI of PLZF in hepatic NKT cells is shown. n=5, $p<0.05$, two-way ANOVA. (R, S) T-bet, Foxp3 and RORγ$^{+}$ level of CD4 T cells in the liver or spleen of C57BL/6 mice treated with ABX or H2O. n=5.

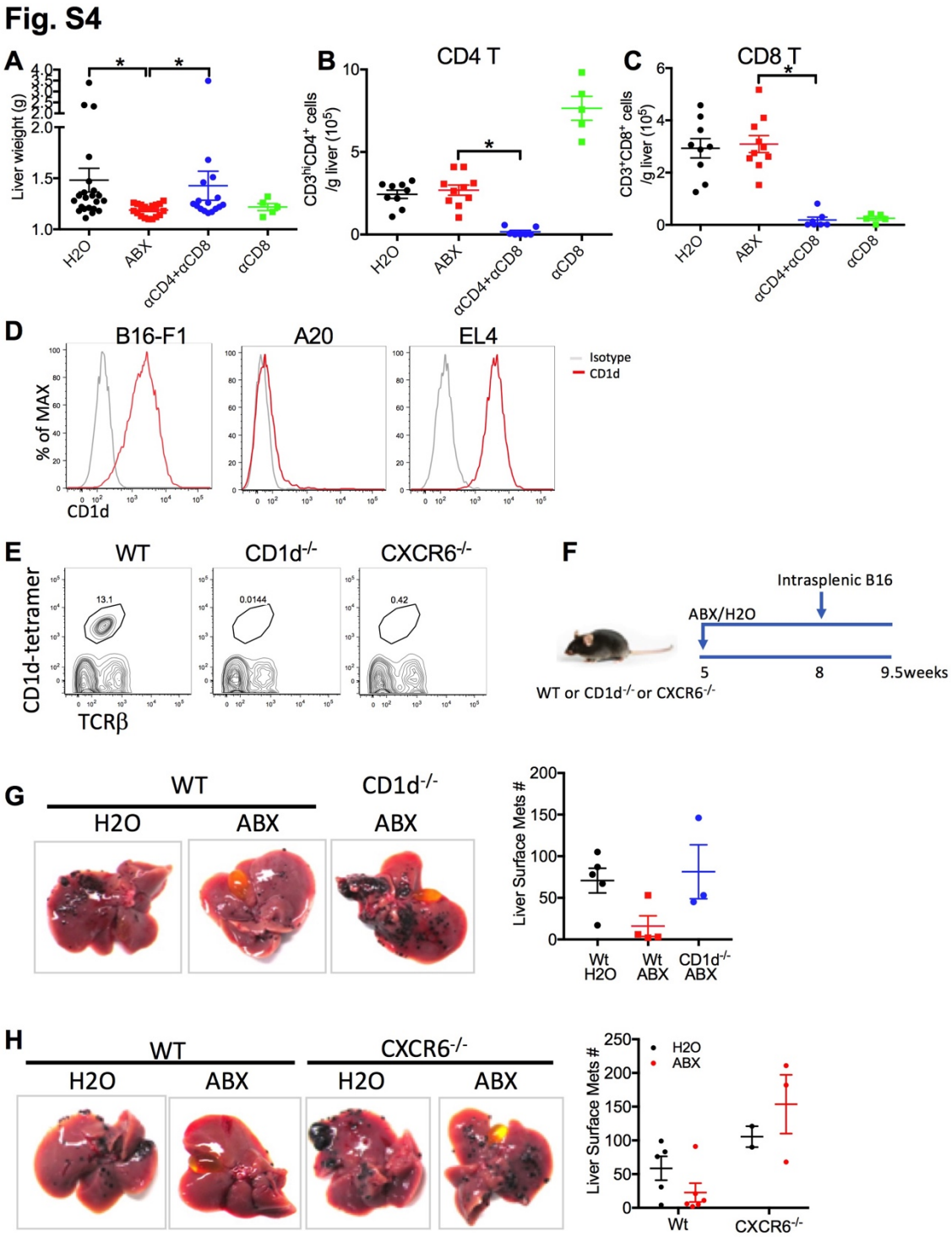


**Fig. S4**

NKT cells mediate gut microbiome-controlled liver tumor growth. (A, B, C) Liver weight, hepatic CD4 T and CD8 T cell levels of the mice received lymphocyte depletion described in Figure 3A. n=16 for H2O, 14 for ABX, 13 for antiCD4+anti-CD8, 5 for anti-CD8. $p<0.05$, one-way ANOVA. (D) CD1d expression level in B16, A20 and EL4 tumor

cells was determined by flow cytometry. (E) Representative of hepatic NKT staining in $CXCR6^{-/-}$ and $CD1d^{-/-}$ mice. (F, G, H) Wildtype, $CXCR6^{-/-}$, and $CD1d^{-/-}$ mice were treated with ABX or H2O for 3 weeks. Then mice were given intrasplenic B16 tumor cell injection. Liver metastases were measured. Representative images are shown. Data represent mean ± SEM of two pooled experiments.

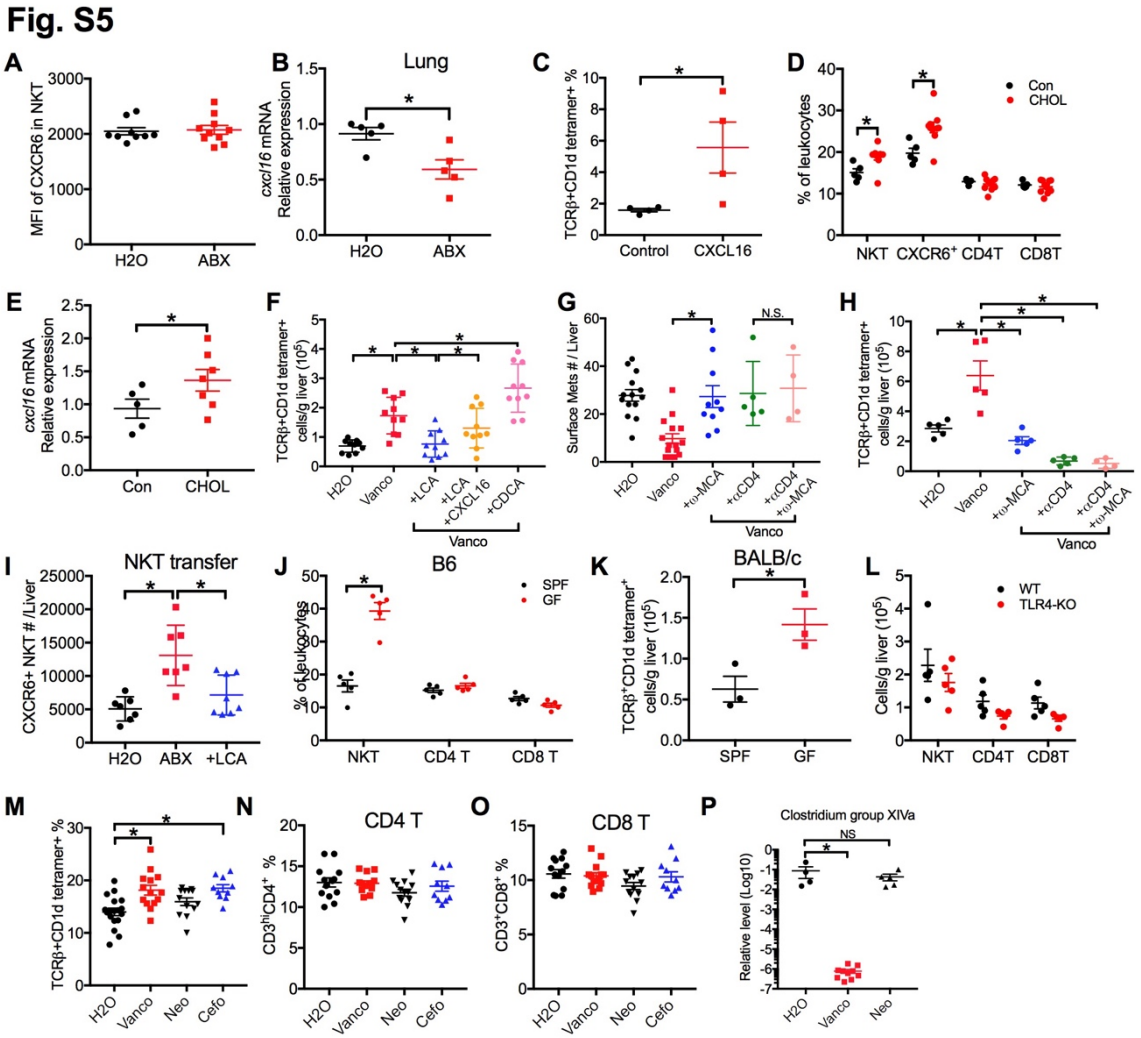


**Fig. S5**

A CXCL16/CXCR6 axis controls hepatic NKT cells. (A) MFI of CXCR6 in hepatic NKT cells from ABX or H2O treated mice. Data represent mean ± SEM of two pooled experiments n=9 for H2O, 10 for ABX. (B) Real-time PCR analysis of CXCL16 mRNA levels in lung tissue from mice treated with ABX or H2O. Data represent mean ± SEM of two pooled experiments n=5, $p<0.05$, Student's t-test. (C) CXCL16-expressing plasmid was delivered into mouse liver by hydrodynamic injection. Hepatic NKT cell levels were measured by flow cytometry. n=4, $p<0.05$, Student's t-test. (D, E) Mice were fed with 2% cholestyramine diet (CHOL) or a control diet (Con) as described in Figure 4D. (D) Frequencies of hepatic NKT, $CXCR6^+$, CD4 T and CD8 T cells were determined. (E) Liver tissue CXCL16 mRNA levels of the mice were measured by real-time PCR. Data represent mean ± SEM of two pooled experiments. n=5 for Con, n=10 for CHOL. $p<0.05$, two-way ANOVA (D) or Student's t-test (E). (F) Hepatic NKT cells were measured from A20 tumor-bearing mice fed with vancomycin (Vanco) or $H_2O$ with the treatment of LCA, CDCA, or with the combination of forced CXCL16 expression by hydrodynamic injection. Data represent mean ± SEM of two pooled experiments. (G, H)

Liver surface tumor counts and Hepatic NKT cells were measured from A20 tumor-bearing mice fed with vancomycin or H2O with the treatment of ω-MCA, anti-CD4 depletion or the combination. (I) $CXCR6^{-/-}$ mice treated with $H_2O$, ABX or with the combination of LCA were given adoptive transfer of NKT-rich cells isolated from wild-type mice. The level of transferred NKT cells was measured by flow cytometry as $TCR\beta^{+}CD1d\text{-}Tetramer^{+}CXCR6^{+}$ population. Data represent mean ± SEM of two pooled experiments. (J, K) Frequencies or absolute number of hepatic NKT cells were measured in Germ-free mice or matched SPF mice on C57BL/6 (J) or BALB/c (K) background. Data represent mean ± SEM of two pooled experiments. (L) Hepatic NKT levels of TLR4 knockout mice or matched wt mice were measured. (M, N, O) Mice were treated with vancomycin, neomycin, cefoparazone or H2O. Frequencies of hepatic NKT, CD4 or CD8 T cells were measured. Data represent mean ± SEM of three pooled experiments. n=18 for H2O, 14 for vancomycin, 14 for neomycin, and 10 for cefoperazone. (P) The stool levels of *Clostridum* Cluster XIVa from single antibiotic treatment were measured by real-time PCR. n=4 for H2O, 10 for vancomycin, 5 for neomycin, $p<0.05$, one-way ANOVA.

**Fig. S6**

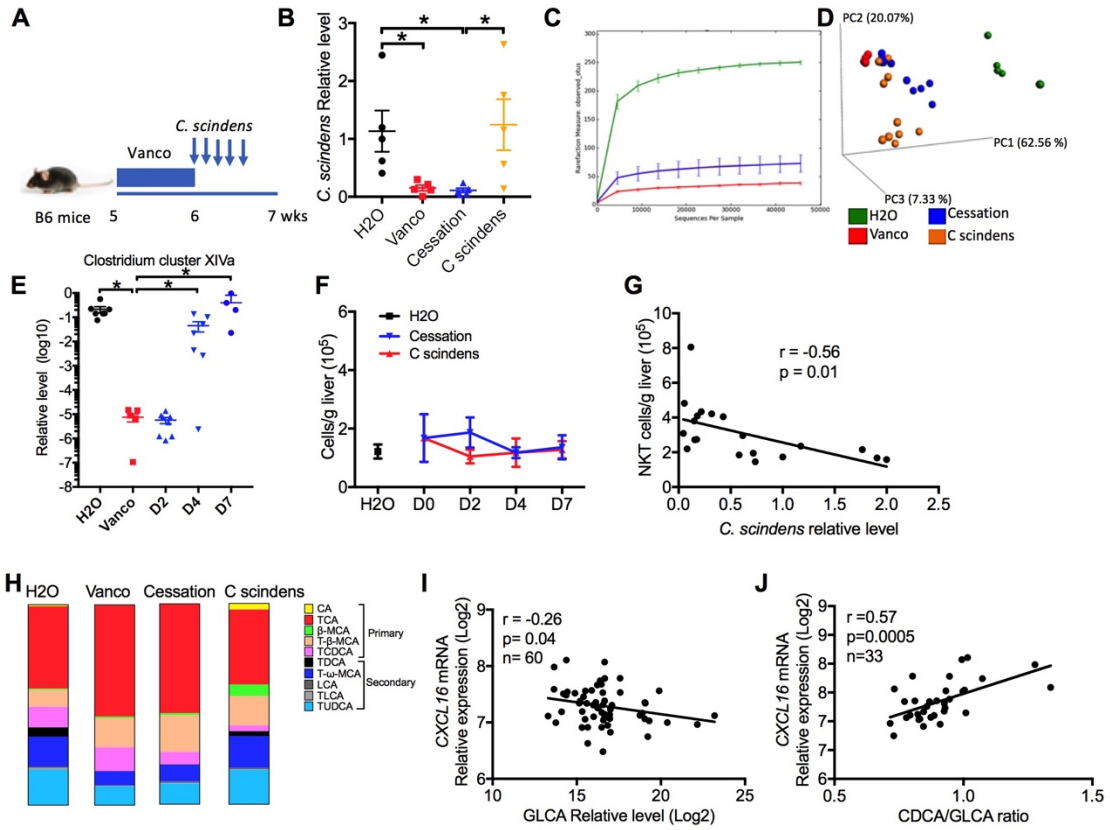


**Fig. S6**

*Clostridium* species-controlled bile acid metabolism regulates hepatic NKT cells. (A, B, C, D, E, F, G, H) Mice were treated with vancomycin for one week. Then vancomycin was stopped, and mice were given oral gavage of *C. scindens* or vehicle (A).Twenty-four hours after gavage, colonization was tested by real-time PCR with *C. scindens*-specific primers (B). Stool bacteria were analyzed by 16S rRNA sequencing. Alpha diversity (C) and beta diversity (D) are shown. In the cessation group, the time course of stool levels of *Clostridium* Cluster XIVa bacteria was measured by real-time PCR(E). Hepatic $CD8^+$ T cell levels under different conditions were measured (F). The correlation between hepatic NKT cells and *C. scindens* levels was tested (G). At the day 2 time point, hepatic bile acid compositions from different conditions were measured (H). (I, J) Correlation between bile acids and CXCL16 expression was tested in non-tumor liver tissues from patients of TIGER cohort. Pearson correlation coefficient test was used.

## References


1. S. Viaud, F. Saccheri, G. Mignot, T. Yamazaki, R. Daillère, D. Hannani, D. P. Enot, C. Pfirschke, C. Engblom, M. J. Pittet, A. Schlitzer, F. Ginhoux, L. Apetoh, E. Chachaty, P.-L. Woerther, G. Eberl, M. Bérard, C. Ecobichon, D. Clermont, C. Bizet, V. Gaboriau-Routhiau, N. Cerf-Bensussan, P. Opolon, N. Yessaad, E. Vivier, B. Ryffel, C. O. Elson, J. Doré, G. Kroemer, P. Lepage, I. G. Boneca, F. Ghiringhelli, L. Zitvogel, The intestinal microbiota modulates the anticancer immune effects of cyclophosphamide. *Science* **342**, 971–976 (2013). doi:10.1126/science.1240537 Medline

2. M. Vétizou, J. M. Pitt, R. Daillère, P. Lepage, N. Waldschmitt, C. Flament, S. Rusakiewicz, B. Routy, M. P. Roberti, C. P. M. Duong, V. Poirier-Colame, A. Roux, S. Becharef, S. Formenti, E. Golden, S. Cording, G. Eberl, A. Schlitzer, F. Ginhoux, S. Mani, T. Yamazaki, N. Jacquelot, D. P. Enot, M. Bérard, J. Nigou, P. Opolon, A. Eggermont, P.-L. Woerther, E. Chachaty, N. Chaput, C. Robert, C. Mateus, G. Kroemer, D. Raoult, I. G. Boneca, F. Carbonnel, M. Chamaillard, L. Zitvogel, Anticancer immunotherapy by CTLA-4 blockade relies on the gut microbiota. *Science* **350**, 1079–1084 (2015). doi:10.1126/science.aad1329 Medline

3. N. Iida, A. Dzutsev, C. A. Stewart, L. Smith, N. Bouladoux, R. A. Weingarten, D. A. Molina, R. Salcedo, T. Back, S. Cramer, R.-M. Dai, H. Kiu, M. Cardone, S. Naik, A. K. Patri, E. Wang, F. M. Marincola, K. M. Frank, Y. Belkaid, G. Trinchieri, R. S. Goldszmid, Commensal bacteria control cancer response to therapy by modulating the tumor microenvironment. *Science* **342**, 967–970 (2013). doi:10.1126/science.1240527 Medline

4. B. Routy, E. Le Chatelier, L. Derosa, C. P. M. Duong, M. T. Alou, R. Daillère, A. Fluckiger, M. Messaoudene, C. Rauber, M. P. Roberti, M. Fidelle, C. Flament, V. Poirier-Colame, P. Opolon, C. Klein, K. Iribarren, L. Mondragón, N. Jacquelot, B. Qu, G. Ferrere, C. Clémenson, L. Mezquita, J. R. Masip, C. Naltet, S. Brosseau, C. Kaderbhai, C. Richard, H. Rizvi, F. Levenez, N. Galleron, B. Quinquis, N. Pons, B. Ryffel, V. Minard-Colin, P. Gonin, J.-C. Soria, E. Deutsch, Y. Loriot, F. Ghiringhelli, G. Zalcman, F. Goldwasser, B. Escudier, M. D. Hellmann, A. Eggermont, D. Raoult, L. Albiges, G. Kroemer, L. Zitvogel, Gut microbiome influences efficacy of PD-1-based immunotherapy against epithelial tumors. *Science* **359**, 91–97 (2018). doi:10.1126/science.aan3706 Medline

5. V. Matson, J. Fessler, R. Bao, T. Chongsuwat, Y. Zha, M.-L. Alegre, J. J. Luke, T. F. Gajewski, The commensal microbiome is associated with anti-PD-1 efficacy in metastatic melanoma patients. *Science* **359**, 104–108 (2018). doi:10.1126/science.aao3290 Medline

6. V. Gopalakrishnan, C. N. Spencer, L. Nezi, A. Reuben, M. C. Andrews, T. V. Karpinets, P. A. Prieto, D. Vicente, K. Hoffman, S. C. Wei, A. P. Cogdill, L. Zhao, C. W. Hudgens, D. S. Hutchinson, T. Manzo, M. Petaccia de Macedo, T. Cotechini, T. Kumar, W. S. Chen, S. M. Reddy, R. Szczepaniak Sloane, J. Galloway-Pena, H. Jiang, P. L. Chen, E. J. Shpall, K. Rezvani, A. M. Alousi, R. F. Chemaly, S. Shelburne, L. M. Vence, P. C. Okhuysen, V. B. Jensen, A. G. Swennes, F. McAllister, E. Marcelo Riquelme Sanchez, Y. Zhang, E. Le Chatelier, L. Zitvogel, N. Pons, J. L. Austin-Breneman, L. E. Haydu, E. M. Burton, J. M. Gardner, E. Sirmans, J. Hu, A. J. Lazar, T. Tsujikawa, A. Diab, H. Tawbi, I. C. Glitza, W. J. Hwu, S. P. Patel, S. E. Woodman, R. N. Amaria, M. A. Davies, J. E. Gershenwald, P. Hwu, J. E. Lee, J. Zhang, L. M. Coussens, Z. A. Cooper, P. A. Futreal, C. R. Daniel,

N. J. Ajami, J. F. Petrosino, M. T. Tetzlaff, P. Sharma, J. P. Allison, R. R. Jenq, J. A. Wargo, Gut microbiome modulates response to anti-PD-1 immunotherapy in melanoma patients. *Science* **359**, 97–103 (2018). doi:10.1126/science.aan4236 Medline

7. S. Yoshimoto, T. M. Loo, K. Atarashi, H. Kanda, S. Sato, S. Oyadomari, Y. Iwakura, K. Oshima, H. Morita, M. Hattori, K. Honda, Y. Ishikawa, E. Hara, N. Ohtani, Obesity-induced gut microbial metabolite promotes liver cancer through senescence secretome. *Nature* **499**, 97–101 (2013). doi:10.1038/nature12347 Medline

8. D. H. Dapito, A. Mencin, G.-Y. Gwak, J.-P. Pradere, M.-K. Jang, I. Mederacke, J. M. Caviglia, H. Khiabanian, A. Adeyemi, R. Bataller, J. H. Lefkowitch, M. Bower, R. Friedman, R. B. Sartor, R. Rabadan, R. F. Schwabe, Promotion of hepatocellular carcinoma by the intestinal microbiota and TLR4. *Cancer Cell* **21**, 504–516 (2012). doi:10.1016/j.ccr.2012.02.007 Medline

9. G. Disibio, S. W. French, Metastatic patterns of cancers: Results from a large autopsy study. *Arch. Pathol. Lab. Med.* **132**, 931–939 (2008). Medline

10. C. Ma, A. H. Kesarwala, T. Eggert, J. Medina-Echeverz, D. E. Kleiner, P. Jin, D. F. Stroncek, M. Terabe, V. Kapoor, M. ElGindi, M. Han, A. M. Thornton, H. Zhang, M. Egger, J. Luo, D. W. Felsher, D. W. McVicar, A. Weber, M. Heikenwalder, T. F. Greten, NAFLD causes selective CD4(+) T lymphocyte loss and promotes hepatocarcinogenesis. *Nature* **531**, 253–257 (2016). doi:10.1038/nature16969 Medline

11. T. Eggert, K. Wolter, J. Ji, C. Ma, T. Yevsa, S. Klotz, J. Medina-Echeverz, T. Longerich, M. Forgues, F. Reisinger, M. Heikenwalder, X. W. Wang, L. Zender, T. F. Greten, Distinct Functions of Senescence-Associated Immune Responses in Liver Tumor Surveillance and Tumor Progression. *Cancer Cell* **30**, 533–547 (2016). doi:10.1016/j.ccell.2016.09.003 Medline

12. A. Marabelle, H. Kohrt, I. Sagiv-Barfi, B. Ajami, R. C. Axtell, G. Zhou, R. Rajapaksa, M. R. Green, J. Torchia, J. Brody, R. Luong, M. D. Rosenblum, L. Steinman, H. I. Levitsky, V. Tse, R. Levy, Depleting tumor-specific Tregs at a single site eradicates disseminated tumors. *J. Clin. Invest.* **123**, 2447–2463 (2013). doi:10.1172/JCI64859 Medline

13. F. Geissmann, T. O. Cameron, S. Sidobre, N. Manlongat, M. Kronenberg, M. J. Briskin, M. L. Dustin, D. R. Littman, Intravascular immune surveillance by CXCR6+ NKT cells patrolling liver sinusoids. *PLOS Biol.* **3**, e113 (2005). doi:10.1371/journal.pbio.0030113 Medline

14. C. H. Kim, E. J. Kunkel, J. Boisvert, B. Johnston, J. J. Campbell, M. C. Genovese, H. B. Greenberg, E. C. Butcher, Bonzo/CXCR6 expression defines type 1-polarized T-cell subsets with extralymphoid tissue homing potential. *J. Clin. Invest.* **107**, 595–601 (2001). doi:10.1172/JCI11902 Medline

15. Y. J. Lee, K. L. Holzapfel, J. Zhu, S. C. Jameson, K. A. Hogquist, Steady-state production of IL-4 modulates immunity in mouse strains and is determined by lineage diversity of iNKT cells. *Nat. Immunol.* **14**, 1146–1154 (2013). doi:10.1038/ni.2731 Medline

16. L. A. Pobezinsky, R. Etzensperger, S. Jeurling, A. Alag, T. Kadakia, T. M. McCaughtry, M. Y. Kimura, S. O. Sharrow, T. I. Guinter, L. Feigenbaum, A. Singer, Let-7 microRNAs target the lineage-specific transcription factor PLZF to regulate terminal NKT cell

differentiation and effector function. *Nat. Immunol.* **16**, 517–524 (2015). doi:10.1038/ni.3146 Medline

17. K. Atarashi, T. Tanoue, T. Shima, A. Imaoka, T. Kuwahara, Y. Momose, G. Cheng, S. Yamasaki, T. Saito, Y. Ohba, T. Taniguchi, K. Takeda, S. Hori, I. I. Ivanov, Y. Umesaki, K. Itoh, K. Honda, Induction of colonic regulatory T cells by indigenous Clostridium species. *Science* **331**, 337–341 (2011). doi:10.1126/science.1198469 Medline

18. E. Vivier, S. Ugolini, D. Blaise, C. Chabannon, L. Brossay, Targeting natural killer cells and natural killer T cells in cancer. *Nat. Rev. Immunol.* **12**, 239–252 (2012). doi:10.1038/nri3174 Medline

19. M. Terabe, J. A. Berzofsky, The role of NKT cells in tumor immunity. *Adv. Cancer Res.* **101**, 277–348 (2008). doi:10.1016/S0065-230X(08)00408-9 Medline

20. M. Terabe, J. A. Berzofsky, in *Encyclopedia of Immunobiology*, M. J. H. Ratcliffe, Ed. (Elsevier, 2016), vol. 4, pp. 460-469.

21. D. Y. Wu, N. H. Segal, S. Sidobre, M. Kronenberg, P. B. Chapman, Cross-presentation of disialoganglioside GD3 to natural killer T cells. *J. Exp. Med.* **198**, 173–181 (2003). doi:10.1084/jem.20030446 Medline

22. K. H. Sonoda, M. Exley, S. Snapper, S. P. Balk, J. Stein-Streilein, CD1-reactive natural killer T cells are required for development of systemic tolerance through an immune-privileged site. *J. Exp. Med.* **190**, 1215–1226 (1999). doi:10.1084/jem.190.9.1215 Medline

23. M. J. Smyth, K. Y. T. Thia, S. E. A. Street, E. Cretney, J. A. Trapani, M. Taniguchi, T. Kawano, S. B. Pelikan, N. Y. Crowe, D. I. Godfrey, Differential tumor surveillance by natural killer (NK) and NKT cells. *J. Exp. Med.* **191**, 661–668 (2000). doi:10.1084/jem.191.4.661 Medline

24. F. Balkwill, Cancer and the chemokine network. *Nat. Rev. Cancer* **4**, 540–550 (2004). doi:10.1038/nrc1388 Medline

25. T. Shimaoka, N. Kume, M. Minami, K. Hayashida, H. Kataoka, T. Kita, S. Yonehara, Molecular cloning of a novel scavenger receptor for oxidized low density lipoprotein, SR-PSOX, on macrophages. *J. Biol. Chem.* **275**, 40663–40666 (2000). doi:10.1074/jbc.C000761200 Medline

26. S. I. Sayin, A. Wahlström, J. Felin, S. Jäntti, H.-U. Marschall, K. Bamberg, B. Angelin, T. Hyötyläinen, M. Orešič, F. Bäckhed, Gut microbiota regulates bile acid metabolism by reducing the levels of tauro-beta-muricholic acid, a naturally occurring FXR antagonist. *Cell Metab.* **17**, 225–235 (2013). doi:10.1016/j.cmet.2013.01.003 Medline

27. Y. Zhang, C. D. Klaassen, Effects of feeding bile acids and a bile acid sequestrant on hepatic bile acid composition in mice. *J. Lipid Res.* **51**, 3230–3242 (2010). doi:10.1194/jlr.M007641 Medline

28. C. Staley, A. R. Weingarden, A. Khoruts, M. J. Sadowsky, Interaction of gut microbiota with bile acid metabolism and its influence on disease states. *Appl. Microbiol. Biotechnol.* **101**, 47–64 (2016). Medline

29. T. Olszak, D. An, S. Zeissig, M. P. Vera, J. Richter, A. Franke, J. N. Glickman, R. Siebert, R. M. Baron, D. L. Kasper, R. S. Blumberg, Microbial exposure during early life has

persistent effects on natural killer T cell function. *Science* **336**, 489–493 (2012). doi:10.1126/science.1219328 Medline

30. C. M. Theriot, A. A. Bowman, V. B. Young, Antibiotic-Induced Alterations of the Gut Microbiota Alter Secondary Bile Acid Production and Allow for Clostridium difficile Spore Germination and Outgrowth in the Large Intestine. *MSphere* **1**, e00045-15 (2016). doi:10.1128/mSphere.00045-15 Medline

31. J. M. Ridlon, D. J. Kang, P. B. Hylemon, Bile salt biotransformations by human intestinal bacteria. *J. Lipid Res.* **47**, 241–259 (2006). doi:10.1194/jlr.R500013-JLR200 Medline

32. C. G. Buffie, V. Bucci, R. R. Stein, P. T. McKenney, L. Ling, A. Gobourne, D. No, H. Liu, M. Kinnebrew, A. Viale, E. Littmann, M. R. M. van den Brink, R. R. Jenq, Y. Taur, C. Sander, J. R. Cross, N. C. Toussaint, J. B. Xavier, E. G. Pamer, Precision microbiome reconstitution restores bile acid mediated resistance to Clostridium difficile. *Nature* **517**, 205–208 (2015). doi:10.1038/nature13828 Medline

33. S. Bhowmik, H.-P. Chiu, D. H. Jones, H.-J. Chiu, M. D. Miller, Q. Xu, C. L. Farr, J. M. Ridlon, J. E. Wells, M.-A. Elsliger, I. A. Wilson, P. B. Hylemon, S. A. Lesley, Structure and functional characterization of a bile acid 7α dehydratase BaiE in secondary bile acid synthesis. *Proteins* **84**, 316–331 (2016). doi:10.1002/prot.24971 Medline

34. J. Chaisaingmongkol, A. Budhu, H. Dang, S. Rabibhadana, B. Pupacdi, S. M. Kwon, M. Forgues, Y. Pomyen, V. Bhudhisawasdi, N. Lertprasertsuke, A. Chotirosniramit, C. Pairojkul, C. U. Auewarakul, T. Sricharunrat, K. Phornphutkul, S. Sangrajrang, M. Cam, P. He, S. M. Hewitt, K. Ylaya, X. Wu, J. B. Andersen, S. S. Thorgeirsson, J. J. Waterfall, Y. J. Zhu, J. Walling, H. S. Stevenson, D. Edelman, P. S. Meltzer, C. A. Loffredo, N. Hama, T. Shibata, R. H. Wiltrout, C. C. Harris, C. Mahidol, M. Ruchirawat, X. W. Wang; TIGER-LC Consortium, Common Molecular Subtypes Among Asian Hepatocellular Carcinoma and Cholangiocarcinoma. *Cancer Cell* **32**, 57–70.e3 (2017). doi:10.1016/j.ccell.2017.05.009 Medline

35. A. Kurioka, L. J. Walker, P. Klenerman, C. B. Willberg, MAIT cells: New guardians of the liver. *Clin. Transl. Immunology* **5**, e98 (2016). doi:10.1038/cti.2016.51 Medline

36. L. Van Kaer, alpha-Galactosylceramide therapy for autoimmune diseases: Prospects and obstacles. *Nat. Rev. Immunol.* **5**, 31–42 (2005). doi:10.1038/nri1531 Medline

37. C. Ma, T. Kapanadze, J. Gamrekelashvili, M. P. Manns, F. Korangy, T. F. Greten, Anti-Gr-1 antibody depletion fails to eliminate hepatic myeloid-derived suppressor cells in tumor-bearing mice. *J. Leukoc. Biol.* **92**, 1199–1206 (2012). doi:10.1189/jlb.0212059 Medline

38. A. Limmer, J. Ohl, C. Kurts, H.-G. Ljunggren, Y. Reiss, M. Groettrup, F. Momburg, B. Arnold, P. A. Knolle, Efficient presentation of exogenous antigen by liver endothelial cells to CD8+ T cells results in antigen-specific T-cell tolerance. *Nat. Med.* **6**, 1348–1354 (2000). doi:10.1038/82161 Medline